ANNUAL REVIEWS

Annual Review of Analytical Chemistry

Advances and Emerging Medical Applications of Direct Mass Spectrometry Technologies for Tissue Analysis

Mary E. King,[1,2] Monica Lin,[1] Meredith Spradlin,[1] and Livia S. Eberlin[2]

[1]Department of Chemistry, The University of Texas at Austin, Austin, Texas, USA; email: Mary.King@bcm.edu

[2]Department of Surgery, Baylor College of Medicine, Houston, Texas, USA; email: Livia.Eberlin@BCM.edu

Annu. Rev. Anal. Chem. 2023. 16:1–25

First published as a Review in Advance on March 21, 2023

The *Annual Review of Analytical Chemistry* is online at anchem.annualreviews.org

https://doi.org/10.1146/annurev-anchem-061020-015544

Keywords

mass spectrometry imaging, clinical diagnostics, ambient ionization, handheld mass spectrometry–based devices

Abstract

Offering superb speed, chemical specificity, and analytical sensitivity, direct mass spectrometry (MS) technologies are highly amenable for the molecular analysis of complex tissues to aid in disease characterization and help identify new diagnostic, prognostic, and predictive markers. By enabling detection of clinically actionable molecular profiles from tissues and cells, direct MS technologies have the potential to guide treatment decisions and transform sample analysis within clinical workflows. In this review, we highlight recent health-related developments and applications of direct MS technologies that exhibit tangible potential to accelerate clinical research and disease diagnosis, including oncological and neurodegenerative diseases and microbial infections. We focus primarily on applications that employ direct MS technologies for tissue analysis, including MS imaging technologies to map spatial distributions of molecules in situ as well as handheld devices for rapid in vivo and ex vivo tissue analysis.

INTRODUCTION

The development of mass spectrometry (MS)–based methods for biomedical applications has generated immense excitement within research and medical communities. With the potential to enhance multiple aspects of clinical workflows, rapid molecular analysis of clinical samples by direct MS technologies has inspired researchers and clinicians to further adapt and implement MS technologies to solve unmet challenges in medicine and healthcare. As research breakthroughs continue to emerge in both ionization methods and new instrumentation that are adaptable to clinical practice, the applications of direct MS technologies are equally expanding. In this review, we highlight new clinical applications of direct MS technologies that have emerged within the last five years (2018–2022) to address diagnostic, prognostic, and therapeutic challenges for a variety of diseases. As represented in **Figure 1**, we showcase recent applications of direct MS technologies for analysis of tissues across selected disease areas, including oncology, neurodegenerative disorders, cardiovascular disease, gynecological conditions, microbial infections, musculoskeletal disorders, and diabetes. Note that by direct MS technology, we refer to techniques used to directly analyze native tissues and biospecimens with MS without extensive sample processing, chemical or physical alteration of the sample, and chromatographic separation. These techniques include matrix-assisted laser desorption ionization (MALDI), secondary ion MS (SIMS), and a variety of ambient ionization MS techniques. Key technical aspects for the technique mentioned are summarized in **Table 1**. As this review focuses on developments regarding MS analyses from tissues and smears, studies involving analysis of biofluids and other biospecimens are not included but covered in other reviews (1, 2). When pertinent, we provide brief perspectives on pioneering opportunities and clinical applications that may benefit from direct MS analysis.

BIOMEDICAL AND DIAGNOSTIC APPLICATIONS

Oncology

Direct MS technologies have been extensively used for characterization of cancerous tissues to probe questions related to tumor pathogenesis and to improve multiple facets of patient management and treatment. In this section, we highlight recent applications of direct MS technologies for enhancing (*a*) preoperative diagnosis and subtyping of tumors, (*b*) prediction of prognosis and treatment response, and (*c*) intraoperative surgical margin evaluation.

Preoperative diagnosis and subtyping. Accurate diagnosis and subtyping of cancers are paramount to guide patient prognosis and therapeutic strategies. Yet, some tumors share highly similar histologic and cytomorphological characteristics, making it difficult to rely on pathological evaluation alone for diagnosis. Morphological similarities between cellular features are often exacerbated in minimally invasive biopsy samples, such as fine needle aspirations (FNAs) (3) or core needles (4), which are collected from suspicious tissue sites or lesions to provide diagnostic information. Often, immunohistochemistry (IHC) and/or other assays are employed to aid in establishing a diagnosis, a prognosis, or molecular subtypes from tissue biopsies for many cancer types, but these methods are time consuming and laborious (5–7). Thus, rapid detection of diagnostic molecular markers via direct MS technologies in preoperative applications could improve treatment management and outcomes of cancer patients.

Direct MS technologies have been increasingly applied to the molecular analysis of minimally invasive tissue biopsies and smears for a wide variety of malignancies (8–13). For instance, Casadonte et al. (8) used MALDI mass spectrometry imaging (MSI) to analyze 219 tissue microarrays collected from needle core biopsies of patients with pancreatic ductal adenocarcinoma

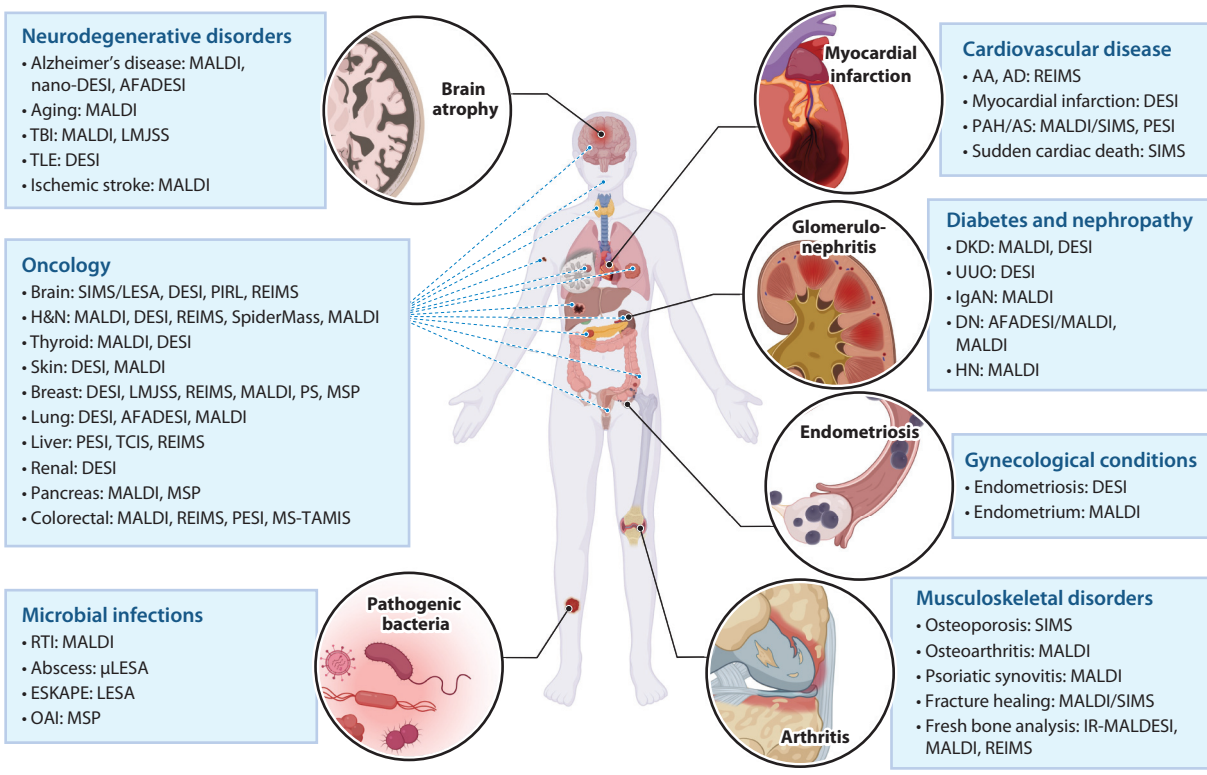

Figure 1

Schematic overview of highlighted and recent clinical applications of direct MS technologies for analysis of tissues and smears described in this review. H&N includes head and neck squamous cell carcinoma and oral squamous cell carcinoma. RTIs include influenza A, *Myobacterium tuberculosis*, *Streptococcus pneumoniae*, and *Staphylococcus aureus*. OAIs include *S. aureus*, *Staphylococcus epidermidis*, *Streptococcus pyogenes*, *Streptococcus agalactiae*, *Kingella kingae*, *Pseudomonas aeruginosa*, *Escherichia coli*, and *Salmonella enterica*. Abbreviations: AA, aortic aneurysm; AD, aortic dissection; AFADESI, air flow–assisted desorption electrospray ionization; AS, atherosclerosis; DESI, desorption electrospray ionization; DKD, diabetic kidney disease; DN, diabetic nephropathy; ESKAPE, *Enterococcus faecium*, *S. aureus*, *Klebsiella pneumoniae*, *Acinetobacter baumannii*, *P. aeruginosa*, and *Enterobacter* species; H&N, head and neck; HN, hypertensive nephrosclerosis; IgAN, immunoglobulin A nephropathy; IR-MALDESI, infrared matrix-assisted laser desorption electrospray ionization; LESA, liquid extraction surface analysis; LMJSS, liquid microjunction surface sampling; MALDI, matrix-assisted laser desorption ionization; MS, mass spectrometry; MSP, MasSpec Pen; OAI, osteoarthritic infection; PAH, pulmonary arterial hypertension; PESI, probe electrospray ionization; PIRL, picosecond infrared laser; PS, paper spray; REIMS, rapid evaporative ionization mass spectrometry; RTI, respiratory tract infection; SIMS, secondary ion mass spectrometry; TAMIS, transanal minimally invasive surgery; TBI, traumatic brain injury; TCIS, tip-contact sampling/ionization; TLE, temporal lobe epilepsy; UUO, unilateral ureteral obstruction. Figure adapted from images created with BioRender.com.

(PDAC; $n = 93$) or pancreatic neuroendocrine tumors (PNETs; $n = 126$). These tumor subtypes are difficult to distinguish histologically from minimally invasive biopsy material but have vastly different prognoses and treatment plans. Linear discriminant analysis (LDA) was used to train a predictive model based on 46 detected peptides from 135 samples, yielding an accuracy of 97% for discriminating tumor subtypes (**Figure 2*c***). Among the features, tumor necrosis factor receptor and tubulins were determined to be predictive of PDAC. Interestingly, overexpression of these molecules has been linked to poorer outcomes in patients with PDAC. In a validation set of 84 samples, 98% accuracy was achieved for distinguishing PDAC from PNETs, further highlighting the potential of the method to improve diagnosis and care for patients.

Table 1 Overview of relevant analytical metrics for direct MS techniques highlighted in this review

Technique	Sampling conditions	Extraction/ desorption mechanism	Ionization mechanism	Spatial resolution[a]	Sample preparation and compatibility	Molecular coverage[b]	Notable references
MS imaging							
MALDI	High vacuum	Laser desorption	Vibrational excitation of matrix	10–100 μm (5 μm) (98)	Tissue sectioning, matrix application, enzymatic digestion;[c] ex vivo/in situ	Metabolites, lipids, glycans, peptides, proteins	99–102
SIMS	High vacuum	Ion beam ablation	Secondary ionization	0.1–10 μm (100 nm) (103)	Tissue sectioning, dehydration/ freeze-drying; ex vivo/in situ	Elements, metabolites, lipids	104–106
AFADESI	Ambient	Liquid extraction	ESI	150–200 μm (100 μm) (107)	Tissue sectioning; ex vivo/in situ	Metabolites, lipids	108, 109
DESI	Ambient	Liquid extraction	ESI	50–200 μm (20 μm) (110)	Tissue sectioning, tissue washing;[d] ex vivo/in situ	Metabolites, lipids, small peptides, proteins (111)	112, 113
LESA	Ambient	Liquid extraction	ESI	0.3–1 mm (conventional) 110 μm (microLESA) (70)	Tissue sectioning; ex vivo/in situ	Metabolites, lipids, peptides, proteins, protein complexes	114, 115
LMJSS	Ambient	Liquid extraction	ESI	0.4–1 mm (400 μm) (116)	Tissue sectioning; ex vivo/in situ	Metabolites, lipids, peptides, proteins	117, 118
Nano-DESI	Ambient	Liquid extraction	ESI	20–150 μm (10 μm) (119)	Tissue sectioning; ex vivo/in situ	Metabolites, lipids, peptides, proteins, protein complexes (120)	121
Handheld devices							
MasSpec Pen	Ambient	Liquid extraction	Thermal vaporization, ESI, or APCI	1.5–5 mm	None; in vivo/ex vivo	Metabolites, lipids	122
PIRL	Ambient	Laser ablation	Laser excitation	0.5–1 mm	None; in vivo/ex vivo	Metabolites, lipids	46, 123
REIMS	Ambient	Thermal desorption or laser ablation	Chemical/ thermal evaporation	0.5–2 mm	None; in vivo/ex vivo	Metabolites, lipids	124
SpiderMass	Ambient	Laser ablation	Laser excitation	400–500 μm (250 μm) (44)	None; in vivo/ex vivo	Metabolites, lipids	125

Notable references include the original report for each technique and/or recent technical reviews. New advancements for specific metrics are referenced throughout the table.

[a]Values listed are the typical range of spatial resolutions reported in studies for biological tissue analysis followed by the highest achievable resolution that has been reported for each technique in parentheses, if applicable.

[b]Classes of molecules described are limited to biological species detected in tissues and smears.

[c]Required for analysis of glycans.

[d]Required for analysis of proteins.

Abbreviations: AFADESI, air flow–assisted desorption electrospray ionization; APCI, atmospheric pressure chemical ionization; DESI, desorption electrospray ionization; ESI, electrospray ionization; LESA, liquid extraction surface analysis; LMJSS, liquid microjunction surface sampling; MALDI, matrix-assisted laser desorption ionization; MS, mass spectrometry; PIRL, picosecond infrared laser; REIMS, rapid evaporative ionization MS; SIMS, secondary ion MS.

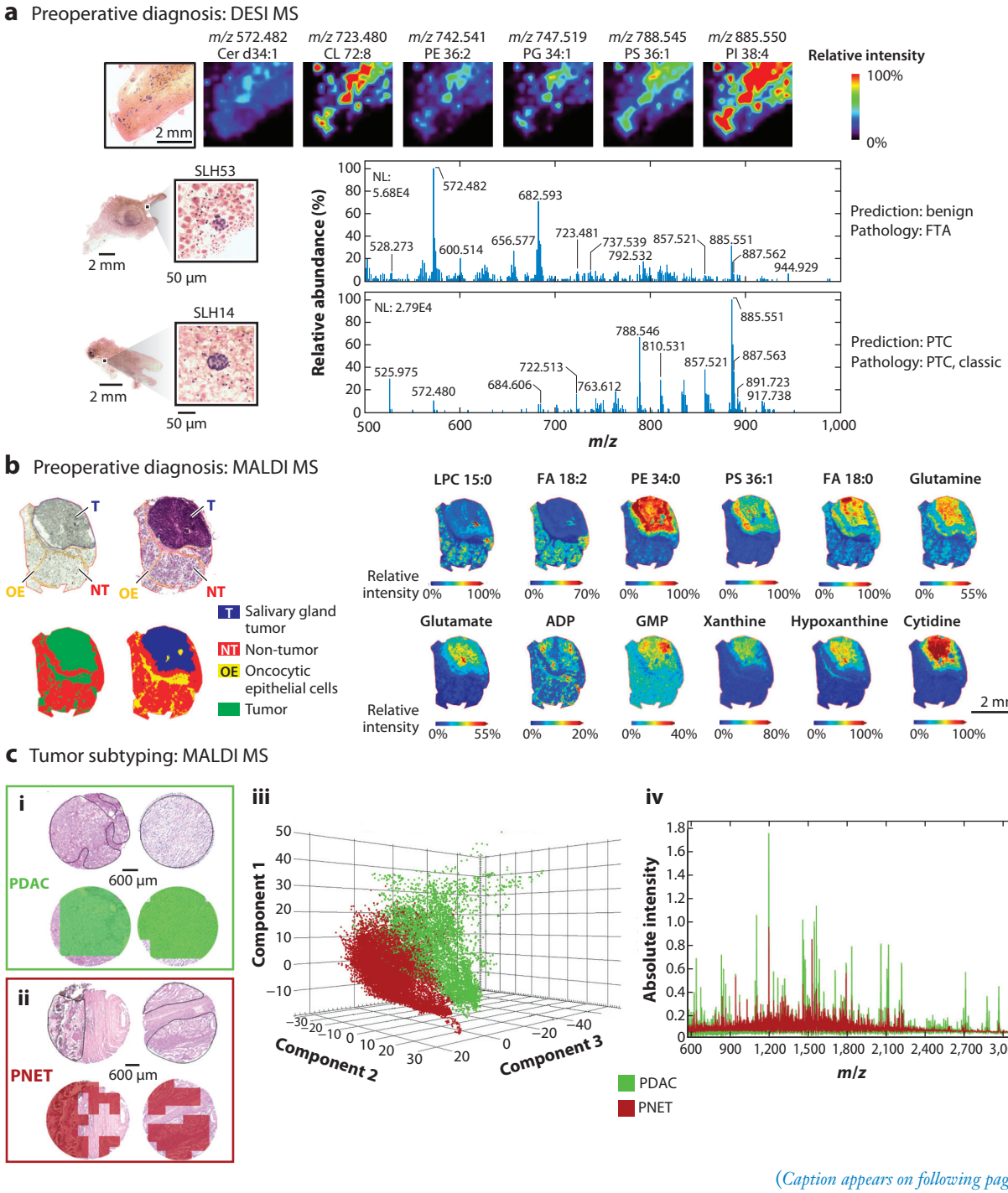

(Caption appears on following page)

Figure 2 (*Figure appears on preceding page*)

Selected direct MS-based technologies for applications in tumor tissue subtyping and preoperative diagnosis. (*a*) DESI MS ion images of a clinical FNA biopsy with corresponding H&E-stained tissues (*top*). Mass spectra with corresponding H&E stains and prediction results for two FNAs (*bottom*). Panel adapted with permission from Reference 11; copyright 2019 NAS. (*b*) Representative MALDI MS ion images of metabolites and lipids from a heterogeneous salivary gland tumor with H&E stain. Panel adapted with permission from Reference 14 (CC BY 4.0). (*c*) H&E-stained tissues overlaid with statistical prediction result for (*i*) PDAC (*green*) and (*ii*) PNET (*red*) tissue microarrays. In the top row of each subpanel, tumor regions are outlined in black within the H&E stains. In the bottom row of each subpanel, the optical image of the H&E stain is overlaid with the LDA prediction results, where green shows pixels predicted as PDAC and red shows pixels predicted as PNET. (*iii*) PCA reveals separation between mass spectra from PDAC (*green*) and PNET (*red*). (*iv*) Averaged mass spectra from PDAC (*green*) and PNET (*red*) tissue microarrays demonstrate qualitative differences in molecular profiles based on pancreatic cancer subtype. Panel adapted with permission from Reference 8; copyright 2019 Wiley-VCH Verlag. Abbreviations: ADP, adenosine diphosphate; Cer, ceramide; CL, cardiolipin; DESI, desorption electrospray ionization; FA, fatty acid; FNA, fine needle aspiration; FTA, follicular thyroid adenoma; GMP, guanosine monophosphate; H&E, hematoxylin and eosin; LDA, linear discriminant analysis; LPC, lysophosphatidylcholine; MALDI, matrix-assisted laser desorption ionization; MS, mass spectrometry; NL, normalization level; PCA, principal component analysis; PDAC, pancreatic ductal adenocarcinoma; PE, phosphatidylethanolamine; PG, phosphatidylglycerol; PI, phosphatidylinositol; PNET, pancreatic neuroendocrine tumor; PS, phosphatidylserine; PTC, papillary thyroid carcinoma.

Studies have also explored the use of MS techniques for direct analysis of FNA biopsies of thyroid nodules to enhance preoperative diagnosis and reduce unnecessary diagnostic surgeries (10–12). For example, DeHoog et al. (11) employed desorption electrospray ionization (DESI) MS in conjunction with lasso and elastic net regression to generate two predictive models based on metabolic markers that distinguished papillary thyroid carcinoma and follicular thyroid carcinoma from benign thyroid (**Figure 2*a***). Important intermediates in metabolic pathways such as malate and succinate associated with dysregulated thyroid cancer metabolism were selected as predictive of follicular thyroid carcinoma tissue. For the papillary thyroid carcinoma model, glycerophospholipid species with a high degree of unsaturations were selected as characteristic of benign tissue. These two models, trained and validated using more than 114,000 tissue mass spectra, were assessed on a test set of 69 clinical FNAs, resulting in 93% and 89% accuracy. Importantly, of 19 FNAs analyzed from patients with indeterminate diagnosis who then underwent diagnostic surgery, 17 were correctly classified as benign using the method developed, thus clearly demonstrating the clinical utility for preoperative diagnosis.

For salivary gland tumors, Sommella et al. (14) recently applied MALDI MS to analyze the metabolite and lipid compositions of 22 fresh frozen human parotid tissues from 11 patients with benign salivary gland tumors, including Warthin, pleomorphic adenoma, and chronic sialadenitis types (**Figure 2*b***). Partial least squares-discriminant analysis (PLS-DA) was used to discriminate healthy from tumor tissues from positive and negative ion mode data. Using variable importance in projection scores derived for each mass-to-charge ratio (m/z) value used in the models, hundreds of molecules were selected as predictive of disease state. While cross-validation accuracy was over 92% for the models developed, moderate accuracies of 68–69% were achieved for the test set, which showcases the potential of the technique but also a critical need for further validation. With further investigation using clinical FNAs, MALDI MS could be established as a potentially valuable tool for preoperative diagnosis of salivary gland neoplasms.

Predicting prognosis and therapeutic response. The unique spatial heterogeneity and chemical complexity of the tumor tissue microenvironment is one of the most significant obstacles in the development of personalized cancer treatments for patients (15). Direct MS profiling and imaging techniques are uniquely suited to help address this fascinating challenge by enabling spatially targeted molecular analysis of heterogeneous tissues. To this end, MSI has been applied in many studies to identify biomarkers that are predictive of patient risk, tumor progression, and therapy response for multiple cancers.

In a recent study by Martin et al. (16), MALDI MSI was employed to perform untargeted proteomic analysis of 276 colon cancer biopsies and investigate the utility of tumor-specific peptide signatures for predicting disease metastasis. Given the complexity of MSI data, the data set was restricted to the top 130 most abundant peptides. Using these data, four different machine learning algorithms were tested separately to ensure robust patient classification. Three of the fitted models predicted the occurrence of distant metastasis in a test set with high accuracies from 92% to 98%, a remarkable result with promising implications for patient care. Further, unsupervised statistical analysis of the unrestricted data set allowed identification of two peptide ions (m/z 1,821.8 and m/z 1,303.6) linked to CK15 and collagen alpha-1 (III) chain that were significantly associated with shorter overall survival.

In another study, air flow–assisted (AFA) DESI MSI was used by Zhang et al. (17) to identify metabolite and phospholipid markers associated with mutation of the epidermal growth factor receptor (*EGFR*) driver oncogene in treatment-naïve non-small cell lung cancer (NSCLC) and adjacent normal tissues acquired postoperatively. *EGFR*-mutated adenocarcinoma samples ($n = 17$) presented spatial enrichment of the phospholipids PE(16:0), PE(18:2), and PC(16:0/18:2) relative to nonmutated samples ($n = 10$). Multivariate analysis enabled classification of *EGFR*-wild-type and *EGFR*-mutated tissues with a diagnostic sensitivity of 82.3% and 80%, respectively, suggesting that the lipid markers might be useful in identifying patients who will benefit from *EGFR*-targeted therapies, although further validation is needed with larger sample sets. In a different study performed to identify predictive markers of therapy response in NSCLC, Berghmans et al. (18) applied MALDI MSI to investigate the spatial peptidomic profiles of formalin-fixed paraffin-embedded (FFPE) lung tissue biopsies collected from 25 patients who later underwent immunotherapy and responded ($n = 9$) or did not respond ($n = 18$) to treatment. The authors identified three peptides, neutrophil defensins 1, 2, and 3, as potential predictive biomarkers of positive response to anti-PD-(L)1 treatment. Validation was performed through IHC staining and quantitation of total neutrophil defensin expression in the same biopsy tissue sections after imaging. Statistical analysis revealed that a patient could be classified as a responder when at least 2% of tumor or immune cells expressed neutrophil defensins, illustrating that the peptides identified may be promising for guiding patient stratification.

Another intriguing prognostic application of MALDI MSI is the spatiochemical interrogation of ancestry-specific disparities in cancer incidence and mortality (19, 20). Rujchanarong et al. (20) recently implemented MALDI MSI to define *N*-glycosylation patterns in normal breast tissue microarrays, correlating the observed glycan profiles to a variety of socioeconomic factors underlying differential breast cancer risk in Black ($n = 43$) and White ($n = 43$) women. For example, the glycan peak at m/z 2,012, identified as Hex5dHex1HexNAc5, was present at higher intensities in breast tissue of White women relative to Black women but was significantly less abundant in obese patients compared to those with a normal body mass index regardless of ancestry. Additional analysis of a breast cancer progression tissue microarray showed that the same peak was elevated in metastatic cores relative to nonmetastatic cores, suggesting that N-linked glycosylation may contribute to ancestry-specific differences in breast cancer risk.

To expand the molecular coverage of prognostic biomarker studies, recent studies have applied multiple techniques for metabolomic, proteomic, and/or genomic phenotyping of tumor tissues. Meurs et al. (21) designed a multimodal approach consisting of high-resolution SIMS followed by spatially targeted liquid extraction surface analysis tandem MS (LESA MS/MS) analysis of the same tissue section. The method was applied to classify six pediatric brain tumor tissues based on whether or not the patient experienced disease relapse after therapy. Complementary MS data sets acquired through the sequential analyses were fused and subjected to PLS-DA, achieving a modest goodness-of-prediction of 0.6375 for relapse risk classification. Sun et al. (22) explored steroid

hormone sulfation in adrenocortical carcinoma biopsies from 72 patients using MALDI MSI, IHC staining, DNA isolation and sequencing, and transmission electron microscopy performed on serial FFPE tissue sections. The relative abundances of estradiol sulfate and estrone-3-sulfate measured by MALDI, as well as the expression of sulfotransferase SULT2A1 quantified through IHC and messenger RNA (mRNA) sequencing, positively correlated with favorable prognosis. An additional sulfated derivative, estradiol-17B 3,17-disulfate, was present only in tumor samples with the poorest overall survival. In a later study, the same authors (23) explored the prognostic utility of native glycan fragments in 109 PDAC FFPE tissues by developing a novel imaging workflow that does not require enzymatic digestion prior to *N*-glycan analysis. Using Kaplan-Meir survival analysis, the researchers found that 10 glycan fragments were significantly associated with a favorable patient outcome when present at high abundances in tumor regions, while another six were significantly associated with poor patient outcome. Two tumor-specific fragments (dHexPenHexAc and dHexHexHexAMe) were identified as independent survival prognostic markers when integrated with tumor stage. Further validation of the molecular species reported in these exploratory studies might have utility in guiding treatment decision making for multiple cancers.

Intraoperative tissue analysis and surgical margin evaluation. Complete surgical removal of tumors offers survival benefits for many cancers (24). However, traditional means of intraoperative surgical margin evaluation using histopathologic evaluation of frozen sections can be challenging to perform and produce subjective results. Thus, the development of MS-based technologies that can be performed intraoperatively to detect molecular signatures in tissues from which a prediction of disease state can be rapidly derived and communicated to surgical staff to help guide surgical excision is an area of burgeoning research interest.

DESI MS has been broadly explored for surgical margin evaluation of ex vivo tissues, including more recent studies in oral (25), renal (26), brain (27, 28), and skin (29) cancers. For example, Brown et al. (27) installed a mobile DESI MS platform coupled to a modified linear ion trap mass spectrometer in a neurosurgical operating theater to characterize molecular profiles and monitor *N*-acetylaspartate and 2-hydroxyglutarate, two oncometabolites associated with tumor cell percentage and glioma prognosis, respectively. The researchers employed a method combining full scan analyses to obtain untargeted molecular profiles and MS/MS scans to monitor each oncometabolite on hundreds of glioma tissue smears resected from 49 patients undergoing craniotomies. Using DESI MS to profile a smear in a zigzag pattern enabled completion of sample analysis in approximately three minutes. The authors demonstrated that this approach allows for both evaluation of IDH1/2 mutation status and surgical margins of gliomas on a timescale that may substantially improve patient treatment.

Other ambient ionization MS techniques (30–34) have been evaluated for surgical margin evaluation of ex vivo tissues. Basu et al. (31) recently reported results using liquid microjunction surface sampling (LMJSS) for intraoperative analysis of freshly excised breast cancer surgical margins in the operating room. Excised normal and cancerous tissues from 21 patients with invasive breast cancer were collected and smeared on a glass slide using a squash preparation technique prior to LMJSS analysis. Statistical visualization of the data revealed separation between tumor and normal tissues based on intensities of five candidate lipid biomarkers (**Figure 3*a***), thus showing promise for identification of disease state in excised breast biopsies within four minutes. The same authors had previously refined a MALDI MS protocol that shortened the total sample preparation and analysis time of ex vivo breast and glioma surgical specimens from 30+ to 5 min (35), further showing the value of direct MS techniques for ex vivo analysis of surgical specimens within the surgical suite.

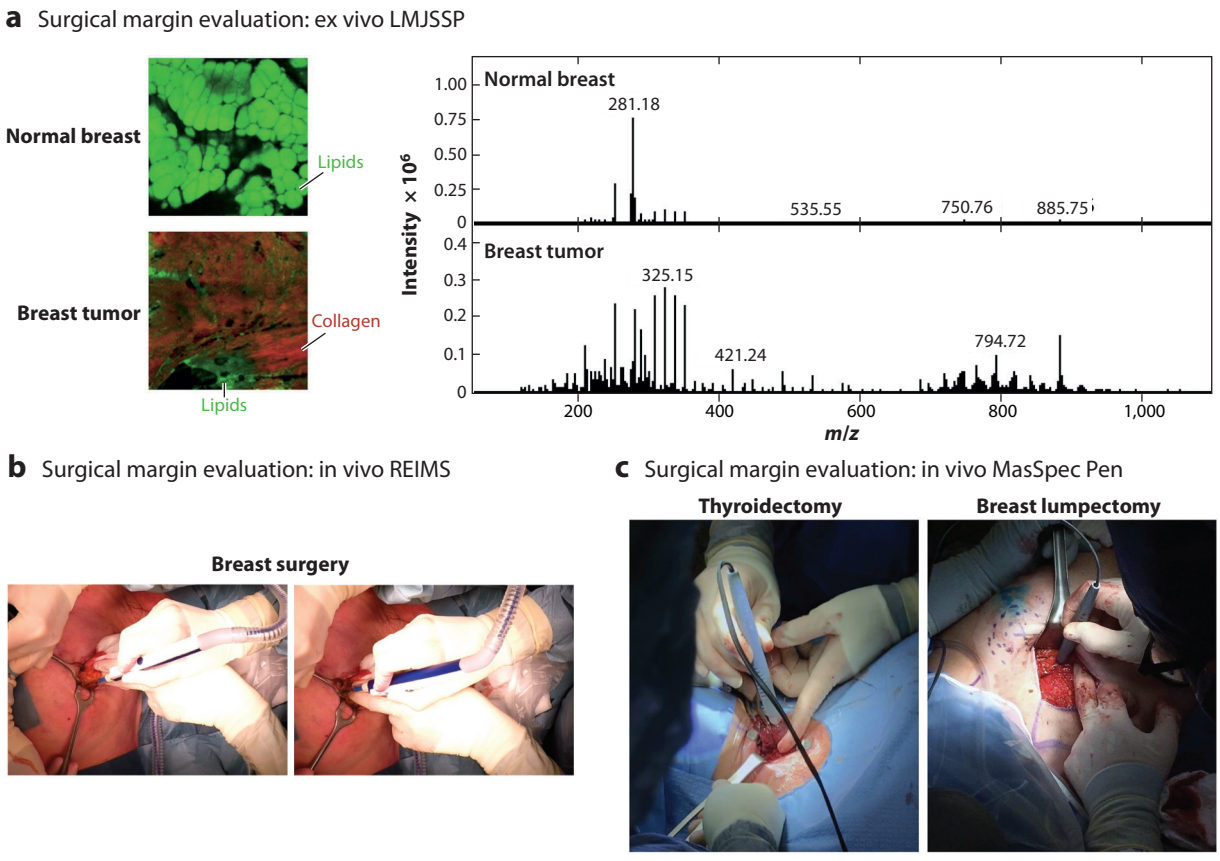

Figure 3

Surgical applications of direct MS-based technologies for in vivo and ex vivo use. (*a*) Stimulated Raman scattering images of lipids in adipocytes (*green*), second-harmonic generation images of collagen (*orange*), and corresponding LMJSS mass spectra for normal breast and breast tumors. Panel adapted with permission from Reference 31 (CC BY 4.0). (*b*) Use of REIMS for in vivo analysis of stromal (*left*) and adipose (*right*) breast tissue during a breast conserving surgery. Panel adapted with permission from Reference 40 (CC BY 4.0). (*c*) In vivo MasSpec Pen analysis during a thyroidectomy (*left*) and a breast lumpectomy (*right*). Panel adapted with permission from Reference 41; copyright 2021 American Association for Clinical Chemistry. Abbreviations: LMJSSP, liquid microjunction surface sampling probe; REIMS, rapid evaporative ionization mass spectrometry.

Technologies that integrate the analytical performance of ambient sampling into user-friendly handheld devices coupled to MS have been introduced for ex vivo and/or in vivo tissue analysis and surgical margin evaluation. Rapid evaporative ionization MS (REIMS), for example, has been applied to the analysis of several cancers (36–40), using both electrocautery- and laser-based systems (**Figure 3*b***). Most recently, Vaysse et al. (39) used REIMS and principal component analysis-linear discriminant analysis (PCA-LDA) to discriminate ex vivo oral cavity cancers and soft tissues in 185 profiles from five patients with 96.8% accuracy in leave-one-out cross-validation. The capability to detect low tumor cell concentrations by REIMS was evaluated by testing varying ratios of tumor cells, keratinocytes, and myoblasts within cell pellets to simulate oral cavity cancer margins. Using this approach allowed researchers to predict as few as 10% of tumor cells in the pellets as cancer with 83% sensitivity. To demonstrate feasibility for in vivo analysis, REIMS was used

intraoperatively to analyze in vivo tissues in four patients undergoing partial glossectomy procedures, although evaluation of predictive models on in vivo data was not reported.

The solvent-based MasSpec Pen technology has been recently evaluated for in vivo and ex vivo tissue analysis in 100 human surgeries (41), including breast, pancreatic, and cervical endocrine cases (**Figure 3*c***). More than 700 molecular profiles composed of small metabolites, fatty acids, and lipids were obtained from fresh tissues, consistent with what the authors had previously observed from fresh frozen banked tissues. Importantly, no tissue damage or disruption to pathological workflows following analysis was encountered given the gentle liquid-based extraction employed by the MasSpec Pen. For evaluation of pancreatic cancer surgical margins, predictive results were reported for 64 in vivo and freshly excised tissue analyses collected during 18 pancreatic resections (42). Classifiers built from metabolite and lipid signatures detected from 157 banked pancreatic and biliary tissues were used to predict on the intraoperative data as an independent test, resulting in overall 93% agreement with histopathology evaluation. Interestingly, the authors showed that including a subset of randomly selected in vivo and ex vivo data into training sets improved prediction agreement to 100% on the remainder of the intraoperative data set, indicating that this may be a valuable approach for increasing the generalizability and robustness of predictive models, although further validation is needed. While the approach is highly promising for surgical margin evaluation in vivo, analyses of positive margins are also necessary to further validate the models for pancreatic cancer detection in vivo.

The laser-based SpiderMass technology has been used for in vivo analysis of sarcomas in canine surgeries (43), imaging mouse tissue in situ at 400–500 μm spatial resolution (44), and ex vivo analysis of human tissues (45). In the imaging study, Ogrinc et al. (44) integrated the SpiderMass probe to a robotic arm and a height measurement sensor. The authors tested the system for MSI of the topography of organs from a sacrificed mouse, observing distinct spatial distribution of lipids such as phosphatidylcholines (PCs) when comparing organs such as the brain, heart, and lungs, as expected. More recently, the same group used this system to image ex vivo FFPE tissues prospectively collected from 14 patients with oral tongue squamous cell carcinoma (45). Based on differences in the lipid profiles between tumor and nontumor regions, a PCA-LDA model was generated yielding an accuracy of 83% in fivefold cross-validation. Another laser-based technique, picosecond infrared laser (PIRL) MS, has been applied in ex vivo analysis and molecular subtyping of human pediatric brain cancers (46) and more recently integrated with an optical surgical tracking system (47). In the latter study, Woolman et al. (47) collected 75 mass spectral profiles of muscle and tumor tissues from five xenograft cancer models using PIRL MS. Using a previously built PCA-LDA model to classify the tissues in real time, they achieved 84% accuracy, with misclassifications mainly attributed to a medulloblastoma cell line tumor that produced low signal intensity. Predictive results based on the MS signatures were correlated with the coordinates of the probe, and color-coded pixels representing the predicted class were projected onto an optical image of the tissue surface that was displayed on a screen in the surgical field-of-view. Adaptation of this platform for use with other handheld MS devices that operate in point sampling mode could improve surgical navigation when analyzing several tissue regions.

Toward expanding the use of MS in minimally invasive surgeries, a few MS devices originally developed for open surgeries have been adapted to fit the physical constraints of minimally invasive procedures (48–50). For example, Keating et al. (48) redesigned the MasSpec Pen for use as a drop-in device with the da Vinci Xi robotic surgical system. Design alterations included reducing the MasSpec Pen case and sampling tip size to fit within a trocar and the addition of a graspable fin for use with a robotic system. This device was then used for in vivo tissue analysis during a robotic-assisted porcine surgery. The distinct metabolic and lipid profiles obtained from stomach and liver tissues were used to develop a statistical classifier to distinguish the organs,

yielding 98% accuracy in cross-validation ($n = 63$ mass spectra) (48). Mason et al. (49) have also coupled REIMS with MS transanal minimally invasive surgery (MS-TAMIS) to evaluate its ability to enhance resection of early rectal cancers. First, 266 MS-TAMIS analyses of fresh frozen tissues obtained from 47 patient samples including normal rectal, adenoma, and cancerous tissues were performed. Orthogonal PLS-DA was used to construct a model for distinguishing normal rectal, adenoma, and cancerous tissues based on the detected lipid profiles, resulting in 86.8% accuracy. The performance of MS-TAMIS for in vivo use was then assessed during five human surgeries. After method optimization during the first four surgeries, the model was tested on 100 burns from the fifth surgery, resulting in 90% accuracy. Collectively, these studies demonstrate the capabilities of MS-based devices compatible with minimally invasive surgeries and their promise for implementation in oncology procedures to guide surgical excision.

Neurodegenerative Disorders

The occurrence of neurodegenerative disorders such as dementia, Parkinson's disease, and Alzheimer's disease (AD) is rapidly increasing worldwide in tandem with the growth of aging populations. Extensive research efforts have pinpointed protein misfolding and aggregation as hallmarks and potential common drivers of neurodegeneration. Given the morphological and molecular complexity of the human brain, spatially targeted, direct MS technologies are well suited for studying the metabolic abnormalities associated with cognitive decline in situ.

MALDI has been used in neuroproteomic studies in both animal models and human tissues. Michno et al. (51) recently applied MALDI MSI to probe the morphologic and structural heterogeneity of β-amyloid (Aβ) peptide aggregates in postmortem brain samples collected from human patients with AD and from cognitively unaffected amyloid-positive individuals. The authors identified disease state–specific alterations in Aβ peptide length and structural diversity. The same authors combined ion mobility MALDI MSI with hyperspectral microscopy to investigate age-dependent lipid alterations associated with Aβ plaque growth and maturation in mouse models (52). Interestingly, older mice displayed an increased relative abundance of PI(18:0/22:6) in the plaque periphery relative to the mature core region, suggesting that intraplaque molecular heterogeneity might play a role in AD pathology. In another multiplexed imaging study by Akerman et al. (53), IHC and MALDI were applied to investigate the expression and spatial distribution of neurodegenerative disease-related proteins such as α-synuclein, tau, and Aβ within the epidermal layer of fresh frozen human skin from young and aged individuals. This study was the first to report α-synuclein detection from skin cell nuclei, as confirmed through comparison of IHC staining and nucleic acid immunofluorescence images. Remarkably, α-synuclein has also recently been detected from rat brain tissue using nano-DESI, representing a substantial step forward in the application of ambient MSI to study native proteins and protein complexes (54). Further expanding the molecular scope of AD proteomic studies, Hawkinson et al. (55) improved the detection of fucosylated and sialylated glycans from human brain tissue by reducing the salt concentration of PNGase F buffer used for on-tissue enzymatic digestion prior to MALDI MSI. This modification allowed comprehensive evaluation of spatial changes in N-linked protein glycosylation in mouse and human AD brains relative to age-matched controls. Hypoglycosylation was observed in the hippocampal regions of human AD brains, where *N*-glycans play a critical role in learning and memory formation, relative to age-matched controls. Interestingly, the hippocampal regions of AD mouse brains were characterized by hyperglycosylation compared to healthy controls, warranting further investigation into the spatially heterogeneous role of glucose metabolism in AD. The optimization of MSI platforms to interrogate the expression of neurodegenerative disease-related proteins, both in neuronal and non-neuronal tissues, presents an exciting approach to investigate potential diagnostic and therapeutic markers for related disorders.

As neurodegeneration is a complex and multifactorial process, it is also relevant to identify downstream alterations in endogenous metabolites and lipids that might contribute to disease pathogenesis. For instance, recent work by Pang et al. (56) utilized AFADESI imaging for comprehensive spatial mapping of hundreds of polar small molecules (m/z < 500) in healthy rat brain tissue and in a scopolamine-treated rat brain model, which recapitulates cognitive impairment similar to what is observed in AD (**Figure 4*a***). High molecular coverage was achieved for neurotransmitters involved in central nervous system regulation and function, such as serotonin, dopamine, and histamine, many of which were present at altered abundances in specific microregions of the AD rat brain tissue relative to healthy control samples. In a related xenograft study, age-related metabolic alterations in neurotransmitter systems were demonstrated to enhance therapeutic response to the acetylcholinesterase inhibitor tacrine, one of the few clinically effective treatments for patients with dementia and AD (57).

Characterization of the human brain lipidome and its role in neurodegeneration has been relatively underexplored due to the limited availability of clinically relevant fresh frozen tissues. Although FFPE human brain samples are more widely available, lipid species are typically not consistently detected due to their removal during the paraffin embedding process (58). However, recent work by Harris and colleagues (59) demonstrated a unique approach to successfully detect lipid species from formalin-fixed brain tissues using MALDI MS by incorporating an ammonium formate wash prior to matrix application, unlocking the potential to perform lipid characterization from FFPE human brain samples. Most notably, the method enabled a tenfold increase in the total ion intensity and a fivefold increase in the number of distinct ganglioside species detected. This method has since been applied to explore the spatial relationship between lipid expression and white matter abnormalities identified by magnetic resonance imaging in postmortem human brain samples (60).

Altered phospholipid metabolism has been further interrogated via DESI MSI of human brain tissues from patients with temporal lobe epilepsy (TLE) (61). TLE induces hippocampal scar tissue formation commonly accompanied by progressive cognitive decline, as observed in many primary neurodegenerative disorders. The authors identified 27 distinct lipid ions, predominantly PC and phosphatidylethanolamine (PE) species, that were present at significantly lower relative abundances in the hippocampal regions of TLE brain tissues relative to non-TLE tissues. Similar patterns of lipid reprogramming have also been implicated in spatially targeted MS rodent studies of ischemic stroke (62, 63) and traumatic brain injuries (64), which are associated with an increased risk of developing dementia and Parkinson's disease. As an increasing number of MS studies implicate metabolic reprogramming in neurodegeneration, these findings provide further insight into the spatiochemical mechanisms of neurodegeneration related to aging, injury, or disease.

Microbial Infections

Early detection and targeted therapeutic intervention are crucial for combatting the rising frequency of bacterial, fungal, and viral diseases. MALDI MS is well established as the leading tool for identification of microbes based on spectral matching of fingerprint peptide profiles from microbes to MS databases. Recent studies have expanded the diagnostic capabilities of MALDI for molecular phenotyping of microbial isolates cultured from primary clinical tissues and biofluids. To further minimize the time and sample preparation requirements associated with pathogen identification, novel approaches using handheld MS devices (65–67) have also been applied to rapidly characterize bacterial isolates with little to no sample preparation. Here, we describe innovations in the detection and characterization of microbial diseases directly from human and animal tissue without the need for cultural isolation.

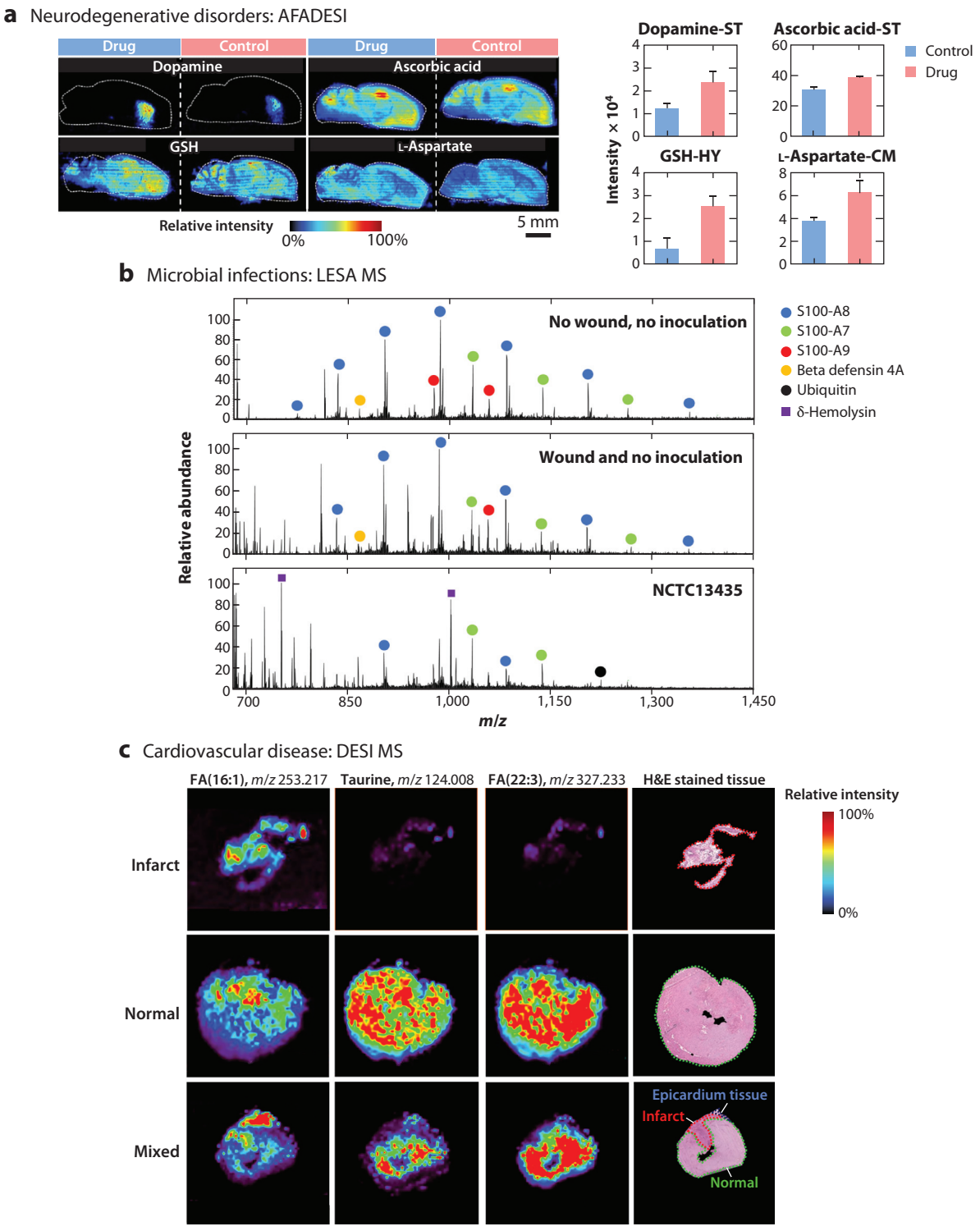

(*Caption appears on following page*)

Figure 4 (*Figure appears on preceding page*)

Selected studies in nononcologic applications of direct MS technologies for disease characterization and diagnosis, including neurodegenerative disorders, microbial infections, and cardiovascular disease. (*a*) AFADESI MS ion images depicting the spatial distribution of metabolites in the rat brains of a scopolamine-treated Alzheimer's model (treated) and healthy controls and corresponding box plots of the relative intensities of each metabolite. Panel adapted with permission from Reference 56; copyright 2021 American Chemical Society. (*b*) LESA MS protein mass spectral profiles obtained from the intact control, wounded control, and "Labskin" samples wounded and infected with *Staphylococcus aureus* NCTC13435. Panel adapted with permission from Reference 69 (CC BY 4.0). (*c*) DESI MS ion images and distributions of various lipid species detected from infarcted myocardium, normal myocardium, and mixed pathologies. Panel adapted with permission from Reference 73; copyright 2018 NAS. Abbreviations: AFADESI, air flow–assisted desorption electrospray ionization; CM, cerebellar medulla; DESI, desorption electrospray ionization; FA, fatty acid; GSH, glutathione; H&E, hematoxylin and eosin; HY, hypothalamus; LESA, liquid extraction surface analysis; MS, mass spectrometry; ST, striatum.

In-depth understanding of host-pathogen interactions in heterogeneous tissues requires comprehensive spatial, temporal, and molecular information. Thus, analysis of microbial infections in tissues presents a relevant application for MSI. Schultz et al. (68) utilized MALDI MSI to investigate lipidomic alterations in murine lung and spleen tissues after respiratory tract infections with *Streptococcus pneumoniae*, *Staphylococcus aureus*, and influenza A virus. The study identified significant alterations in bioactive lipid species involved in modulating immune system response, most notably sphingosine-1-phosphate and ceramide-1-phosphate derivatives. Interestingly, regiospecific accumulation of long-chain ceramide-1-phosphates was observed in both lung and spleen tissues after host coinfection with *S. pneumoniae* and influenza A but not after single infections, suggesting a unique immune response to coinfection that impacts the abundance and distribution of signaling lipids.

The utility of direct MS technologies for microbial identification in clinical tissues is currently limited, as detection of microbes from biospecimens obtained through minimally invasive collection (blood, urine, saliva, etc.) is preferred in most cases. However, a valuable medical application for these technologies is in the point-of-care and rapid diagnosis of pathogens from tissue wounds. An exciting study by Havlikova et al. (69) described the application of LESA MS for proteomic characterization of ESKAPE pathogens, the leading cause of hospital-acquired infections, directly from infected wounds in living three-dimensional skin models (**Figure 4*b***). The top-down approach developed was effective for rapid differentiation of genetically similar strains based on bacterial proteins and enabled detection of human skin proteins including β-defensin, ubiquitin, and S100 calcium-binding proteins. Ryan et al. (70) recently introduced a bottom-up proteomics workflow, deemed microLESA, which incorporates spatially targeted, piezoelectric deposition of trypsin protease guided by autofluorescence microscopy for localized protein microdigestion prior to LESA. With this technique, spatiotemporal proteomic profiling of staphylococcal abscess formation and development in mouse kidney tissues was achieved with a sampling spatial resolution of 110 μm (71). To achieve rapid clinical identification of infectious bacteria, Povilaitis et al. (72) applied the MasSpec Pen to analyze 43 well-characterized strains of eight bacteria species that are common infectious agents of osteoarthritic infections. Five statistical classifiers were built from the 247 molecular profiles obtained for Gram-, species-, and genus-level identification, yielding a mean accuracy of 93.3% considering training and validation sets. The model was then used to predict on an independent test of three surgical specimens, including joint fluid and bone tissue, and matching isolates from patients with osteoarthritic infections. Predictions on biospecimens were accurate for Gram stain-type and genus-level identification, suggesting that the MasSpec Pen may be valuable for microbial identification directly from patient samples.

Cardiovascular Disease

MS techniques have been widely utilized to investigate metabolite and lipid signatures in cardiac diseases such as myocardial infarction (73), pulmonary arterial hypertension (74), and sudden cardiac death (SCD) (75). In particular, MSI of endogenous metabolites and lipids has been performed to monitor disease progression, predict cardiovascular events, and provide new insights into therapeutic interventions (76). For example, Margulis et al. (73) employed DESI MSI along with machine learning algorithms to perform predictions on myocardial pathology based on selected mass spectral features using mouse models (**Figure 4*c***). Consistent with the knowledge that higher levels of polyunsaturated fatty acids (PUFAs) are associated with improved cardiovascular health and outcomes, the MS profiles depicted diminished relative abundances of PUFAs and a few small metabolites detected in infarcted myocardium compared to normally perfused myocardium tissue samples. In addition, depleted levels of glycerophospholipids and elevated relative abundances of monounsaturated and some saturated fatty acids were also observed in the infarcted myocardium.

The potential use of MSI for forensic diagnosis in cardiac disease has been suggested as a potential method for postmortem diagnosis of SCD, a current clinical challenge owing to the lack of reliable biomarkers and undiagnostic morphological evidence collected during pathological evaluation (75). Lou et al. (75) reported the use of SIMS to image SCD-affected and normal mouse myocardium tissues with a remarkable spatial resolution of 200 nm. In the positive ion mode, highly characteristic lipid profiles were observed comparing β-adrenergic receptor activation-induced SCD and normal myocardium tissue samples. Specifically, a decreased relative abundance of various diacylglycerols was observed in the mass spectra from SCD mouse tissue when compared to normal myocardium, while lysoPCs and PC species were detected at an elevated relative abundance. Notably, similar trends in lipid profiling were also observed in human myocardial tissue sections, suggesting that these lipid trends could potentially be used as diagnostic biomarkers for analyzing human SCD cases (75).

Applications of handheld MS devices for cardiovascular disease have recently emerged, including rapid tissue profiling of aortic aneurysms (77) and molecular markers of structural integrity in aortic dissections (78). For example, Davies et al. (77) used REIMS to discriminate between banked 44 aneurysmal and 13 normal aortic tissues with 88.7% accuracy using PLS-DA, showcasing the potential of ambient MS and handheld sampling for aiding intraoperative evaluation and resection of cardiovascular tissues. As a result of successful ex vivo diagnosis of these pathologies, future studies focused on in vivo validation for intraoperative decision making are needed.

Gynecological Conditions

Investigation of gynecological diseases such as endometriosis has been relatively underexplored using direct MS technologies, but this area has gained interest in the last few years. Although endometriosis is a highly prevalent disease, its biological mechanisms are poorly understood, and the condition is often misdiagnosed due to the current unavailability of preoperative diagnostic methods. Using DESI MSI, Feider et al. (79) explored lipid and metabolite markers of 231 ectopic and eutopic endometrial tissues from endometriosis patients (**Figure 5*b***). The study revealed differences in both the relative abundances and spatial distributions detected for a variety of small metabolites, free fatty acids, and lipids. For example, an increased abundance of PS(36:1) was observed within endometriosis lesions, whereas iodide was in higher abundance in eutopic endometrium. Further, although eutopic endometrium tissues presented a homogeneous distribution of endogenous molecules, endometriosis lesions yielded a more heterogeneous distribution of molecular ions with higher signal intensities detected in tissue regions that contained endometrial

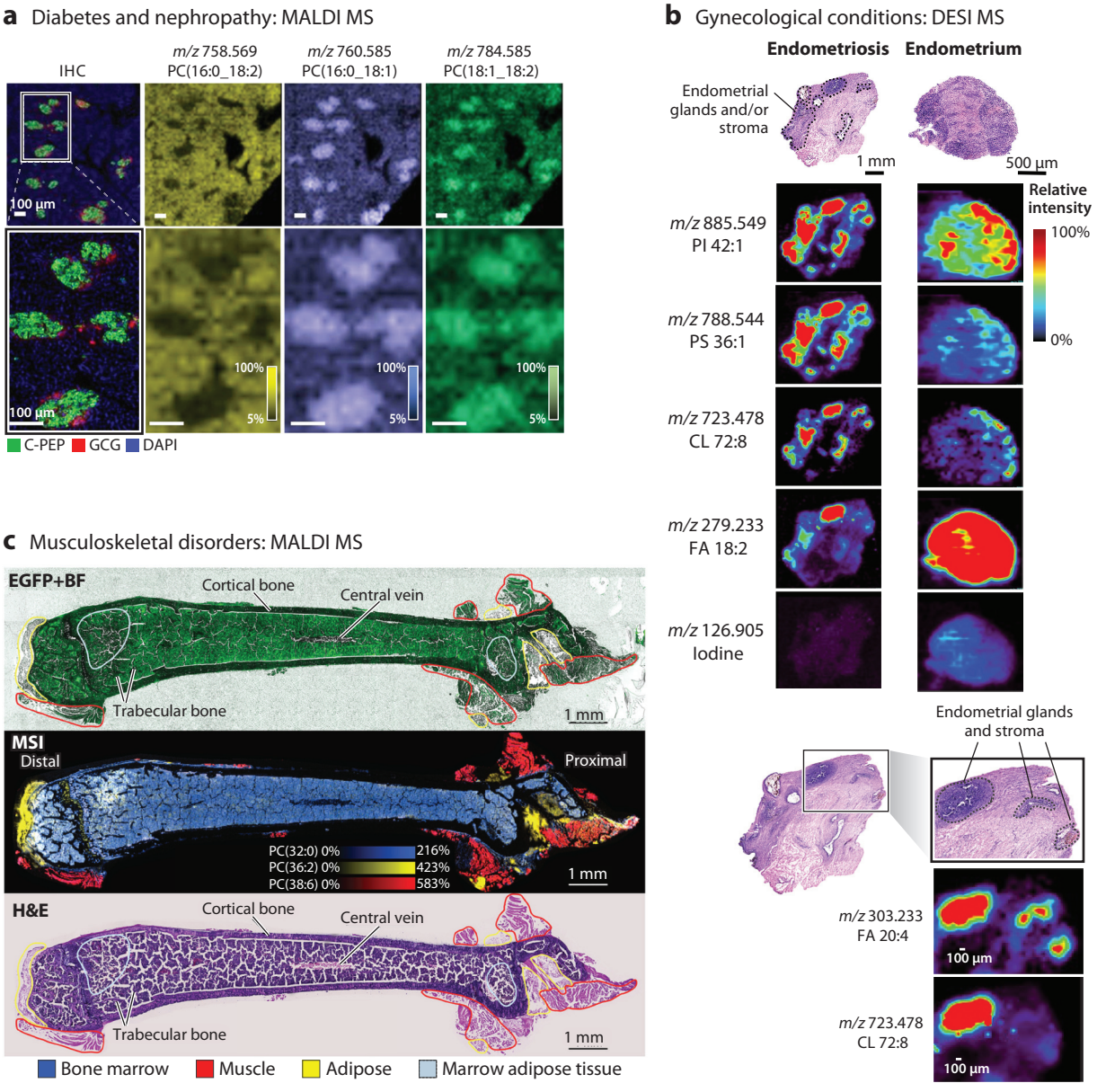

Figure 5

Selected studies in nononcologic applications of direct MS technologies for disease characterization and diagnosis, including diabetes, gynecological conditions, and musculoskeletal disorders. (*a*) Co-registration of immunofluorescence and MALDI MS imaging of pancreatic tissue sections. Ion images depict the spatial distribution for a series of PC ions. Intensity scales are shown in the bottom right of each magnified image in the bottom row. Panel adapted with permission from Reference 89; copyright 2019 Springer Nature. (*b*) DESI MS ion images of eutopic and ectopic endometrial tissues from endometriosis patients with corresponding H&E stains. Panel adapted with permission from Reference 79 (CC BY 4.0). (*c*) Sample preparation for MALDI MS imaging of undecalcified fresh frozen mouse femurs. Differences in bone marrow morphology and signal intensity of biomolecules were dependent on the sample preparation methods. Panel adapted with permission from Reference 87; copyright 2022 American Chemical Society. Abbreviations: BF, bright field; CL, cardiolipin; C-PEP, C-peptide; DESI, desorption electrospray ionization; EGFP, enhanced green fluorescent protein; FA, fatty acid; GCG, glucagon; H&E, hematoxylin and eosin; IHC, immunohistochemistry; MALDI, matrix-assisted laser desorption ionization; MS, mass spectrometry; MSI, MS imaging; PC, phosphatidylcholine; PI, phosphatidylinositol; PS, phosphatidylserine.

glands and stroma. Although preliminary, the study provided new insights into potential biological pathways and alterations in metabolism previously unexplored in endometriosis tissues. New developments toward improving protein molecular coverage have been recently reported to investigate protein distribution in endometriosis tissues. In particular, Lin et al. (80) reported the introduction of a red blood cell lysis buffer washing step applied to MALDI MSI to reduce ion suppression effects from hemoglobin proteins present in blood-rich tissues such as endometrium. This method improved detection of other endogenous proteins directly from tissue sections, such as COX7C and histones in human endometrium, thus enabling future protein imaging studies in endometriosis.

Musculoskeletal Disorders

Recent advances in direct MS technologies have further improved chemical analysis of histologically and molecularly heterogeneous bone tissues. Applications have focused on providing new biological insights and treatment strategies for musculoskeletal disorders including osteoporosis and osteoarthritis (81–84) and bone fracture healing (85). For example, Rocha et al. (82) applied MALDI MSI to identify alterations in lipid profiles of human knee synovium from normal and osteoarthritis-affected patients as well as psoriatic and rheumatoid arthritis tissues. Distinct lipid patterns related to the different conditions were observed, with high abundances of PCs and sphingomyelins correlated to histological regions characterized by vascularization and inflammation within the osteoarthritis-affected synovium compared to healthy synovium, while lower abundances of plasmalogen PEs were detected in osteoarthritis compared to other arthritic conditions. Given the fragile morphology of hard tissues, optimization of sample preparation protocols has been critical to preserve tissue structure prior to MSI (83, 86, 87). For example, Eveque-Mourroux et al. (83) developed a MALDI MSI sample preparation workflow to image metabolites in human osteoarthritis cartilage. The introduction of a heat stabilization protocol prior to snap freezing improved the signal-to-noise ratio of various nucleotides and nucleotide sugars compared to when heat stabilization was not employed. Additionally, an optimized matrix application parameter was found to be critical to prevent compound delocalization within tissue sections and thus differentiate the metabolic profiles of superficial and deep cartilage areas.

Sample processing methods to improve analysis of undecalcified fresh frozen bone tissues, which are prone to cracking, have also been recently reported (86, 87). For example, Good et al. (87) developed a method by which cryofilm-assisted sections of mouse femurs were mounted on conductive slides via adhesive and then subjected to matrix sublimation, resulting in minimized tissue cracks and thus improving MALDI MSI data and downstream microscopy quality (**Figure 5*c***). Using this approach, a variety of endogenous lipids were detected specific to soft tissue structures including bone marrow, adipose, and muscle at 10-μm spatial resolution, whereas no lipid signal was detected from hard tissue such as cortical or trabecular bones. Shorter chain saturated PC(32:0) was abundantly detected in bone marrow, while longer chain PUFA lipids PC(36:2) and PC(38:6) were primarily localized within the adipose and muscle tissue, respectively. Further improvements in the rapid analysis of hard tissues such as bone, cartilage, and bone marrow have also been explored in a study with REIMS (88), in which the use of a CO_2 laser REIMS effectively generated a lipid-rich smoke directly from hard tissues, thus expanding the use of this technology to study bone-related injuries and malignancies.

Diabetes and Nephropathy

Several studies have recently employed direct MS techniques to explore the heterogeneous structures and molecular alterations in tissues damaged by diabetes (89–91) and kidney diseases (92).

For example, Prentice et al. (89) outlined a workflow to coregister MALDI MS and immunofluorescence images to accurately identify cell types in selected subregions of interest in murine and human pancreatic tissues based on their molecular distributions (**Figure 5*a***). The method allowed pancreatic islets containing insulin-producing beta cells to be localized and resolved with a spatial resolution of 30 μm.

In a study by Zhang et al. (90) DESI MSI was used to investigate the spatial distribution of metabolites in the kidneys of mouse models of type 1 diabetes to provide further insights into diabetic kidney disease. Using the bioinformatics platform METASPACE to aid in annotation of metabolites in MSI data (93), researchers identified hundreds of *m/z* values detected in different abundances in diabetic kidney disease mouse models relative to normal controls as metabolites and lipid species. Specifically, the data revealed a notable accumulation of PUFAs but decreased abundance of cardiolipins in the cortical proximal tubules in the diabetic kidney disease mouse models compared to healthy controls, potentially providing insight into disease pathogenesis and key metabolic pathways in diabetes (90).

MSI techniques have also been increasingly applied to spatially resolve histologic structures including the glomeruli, tubuli, and vessels within highly heterogeneous kidney tissue biopsies from patients with nephropathy. MALDI MSI of human kidney biopsies has also been performed recently for improving diagnosis and treatment of diseases that can lead to end-stage renal disease, including immunoglobulin A nephropathy (94), diabetic nephropathy, and hypertensive nephrosclerosis (95). In the latter study, Smith et al. (95) applied MALDI MS to identify new protein biomarkers from human renal biopsies for discriminating diabetic nephropathy from hypertensive nephrosclerosis, which are challenging to distinguish using traditional clinical assays but have different prognoses and therapeutic options. Of four proteins identified as differentially expressed in diabetic nephropathy and hypertensive nephrosclerosis, PGRMC1 and CO3 may also have prognostic value, as they were detected in increased abundance in diabetic nephropathy biopsies with more severe disease.

An impressive project using direct MS technologies among other techniques to study kidney tissues is the Kidney Precision Medicine Project. The project aims at improving understanding of human kidney health and disease by creating a reference kidney atlas that combines comprehensive imaging, transcriptomic, proteomic, and metabolomic information to characterize disease subtypes and identify therapeutic targets (96). As part of this project, Hansen et al. (97) described an approach to identify glomeruli markers in MALDI MSI data along with METASPACE. For instance, a molecule that localized to glomerular regions was identified as CerP(d34:1). Subsequently, a spatial colocalization analysis was performed to identify all other biomolecules that colocalized with CerP(d34:1), revealing 30 molecular markers associated with glomeruli regions. Overall, the continued application of direct MS technologies in the investigation of human kidney disease highlights their promising capabilities as a powerful clinical tool for enabling new discoveries in disease prevention, diagnosis, and prognosis, as well as for potential treatment options.

CONCLUSIONS AND OUTLOOK

Driven largely by pressing clinical obstacles and diagnostic challenges, the field of direct MS techniques has dramatically advanced in the last five years with new applications and developments. We foresee that these MS techniques will continue to be embraced by researchers and clinicians as powerful tools to investigate dysregulated metabolism in biomedical and clinical applications and complement clinical decision making. With further technical refinements and testing, the implementation of ambient ionization MS techniques in the clinic for biomedical applications is imminent. The realization of technical improvements and software capabilities that increase the

robustness, cost-efficiency, and operational ease-of-use will further substantiate the benefits and capabilities of direct MS technologies. If these past five years are an indication of future success, we anticipate that these MS technologies will become indispensable tools for routine diagnostic and clinical use in hospitals around the world.

DISCLOSURE STATEMENT

L.S.E. is an inventor on US Patent No. 10,643,832 and/or other patent applications related to the MasSpec Pen Technology licensed by The University of Texas to MS Pen Technologies, Inc. L.S.E. is a shareholder in MS Pen Technologies, Inc., serves as chief scientific officer and board member for MS Pen Technologies, Inc., is an inventor on patents related to DESI MS Technology licensed by Purdue Research Foundation to Waters Corp., and receives royalties from sales of DESI systems. M.E.K., M.L., and M.S. are not aware of any affiliations, memberships, funding, or financial holdings that might be perceived as affecting the objectivity of this review.

ACKNOWLEDGMENTS

This work was supported by the National Cancer Institute of the US National Institutes of Health, Eli Lilly and Company, Cancer Prevention and Research Institute of Texas, and the Gordon and Betty Moore Foundation. M.L. thanks The University of Texas at Austin for their support with a Provost Graduate Excellence Fellowship.

LITERATURE CITED

1. Swiner DJ, Jackson S, Burris BJ, Badu-Tawiah AK. 2020. Applications of mass spectrometry for clinical diagnostics: the influence of turnaround time. *Anal. Chem.* 92:183–202
2. Pu F, Chiang S, Zhang W, Ouyang Z. 2019. Direct sampling mass spectrometry for clinical analysis. *Analyst* 144:1034–51
3. Gupta S, Dey P. 2021. Diagnostic challenges in the gray-zone lesions of fine-needle aspiration cytology. *CytoJournal* 18:23
4. Neal L, Sandhu NP, Hieken TJ, Glazebrook KN, Mac Bride MB, et al. 2014. Diagnosis and management of benign, atypical, and indeterminate breast lesions detected on core needle biopsy. *Mayo Clin. Proc.* 89:536–47
5. Hicks DG, Tubbs RR. 2005. Assessment of the *HER2* status in breast cancer by fluorescence in situ hybridization: a technical review with interpretive guidelines. *Hum. Pathol.* 36:250–61
6. Yaziji H, Barry T. 2006. Diagnostic immunohistochemistry: What can go wrong? *Adv. Anat. Pathol.* 13:238–46
7. Chrzanowska NM, Kowalewski J, Lewandowska MA. 2020. Use of fluorescence in situ hybridization (FISH) in diagnosis and tailored therapies in solid tumors. *Molecules* 25:1864
8. Casadonte R, Kriegsmann M, Perren A, Baretton G, Deininger S-O, et al. 2019. Development of a class prediction model to discriminate pancreatic ductal adenocarcinoma from pancreatic neuroendocrine tumor by MALDI mass spectrometry imaging. *Proteom. Clin. Appl.* 13:e1800046
9. Lazova R, Smoot K, Anderson H, Powell MJ, Rosenberg AS, et al. 2020. Histopathology-guided mass spectrometry differentiates benign nevi from malignant melanoma. *J. Cutan. Pathol.* 47:226–40
10. Piga I, Capitoli G, Tettamanti S, Denti V, Smith A, et al. 2019. Feasibility study for the MALDI-MSI analysis of thyroid fine needle aspiration biopsies: evaluating the morphological and proteomic stability over time. *Proteom. Clin. Appl.* 13:e1700170
11. DeHoog RJ, Zhang J, Alore E, Lin JQ, Yu W, et al. 2019. Preoperative metabolic classification of thyroid nodules using mass spectrometry imaging of fine-needle aspiration biopsies. *PNAS* 116:21401–8
12. Capitoli G, Piga I, L'Imperio V, Clerici F, Leni D, et al. 2022. Cytomolecular classification of thyroid nodules using fine-needle washes aspiration biopsies. *Int. J. Mol. Sci.* 23:4156

13. Bensussan AV, Lin J, Guo C, Katz R, Krishnamurthy S, et al. 2020. Distinguishing non-small cell lung cancer subtypes in fine needle aspiration biopsies by desorption electrospray ionization mass spectrometry imaging. *Clin. Chem.* 66:1424–33
14. Sommella E, Salviati E, Caponigro V, Grimaldi M, Musella S, et al. 2022. MALDI mass spectrometry imaging highlights specific metabolome and lipidome profiles in salivary gland tumor tissues. *Metabolites* 12:530
15. Gonçalves JPL, Bollwein C, Schwamborn K. 2022. Mass spectrometry imaging spatial tissue analysis toward personalized medicine. *Life* 12:1037
16. Martin B, Gonçalves JPL, Bollwein C, Sommer F, Schenkirsch G, et al. 2021. A mass spectrometry imaging based approach for prognosis prediction in UICC stage I/II colon cancer. *Cancers* 13:5371
17. Zhang M, He J, Li T, Hu H, Li X, et al. 2019. Accurate classification of non-small cell lung cancer (NSCLC) pathology and mapping of *EGFR* mutation spatial distribution by ambient mass spectrometry imaging. *Front. Oncol.* 9:804
18. Berghmans E, Jacobs J, Deben C, Hermans C, Broeckx G, et al. 2020. Mass spectrometry imaging reveals neutrophil defensins as additional biomarkers for anti-PD-(L)1 immunotherapy response in NSCLC patients. *Cancers* 12:863
19. Conroy LR, Stanback AE, Young LEA, Clarke HA, Austin GL, et al. 2021. *In situ* analysis of N-linked glycans as potential biomarkers of clinical course in human prostate cancer. *Mol. Cancer Res.* 19:1727–38
20. Rujchanarong D, Scott D, Park Y, Brown S, Mehta AS, et al. 2022. Metabolic links to socioeconomic stresses uniquely affecting ancestry in normal breast tissue at risk for breast cancer. *Front. Oncol.* 12:876651
21. Meurs J, Scurr DJ, Lourdusamy A, Storer LCD, Grundy RG, et al. 2021. Sequential orbitrap secondary ion mass spectrometry and liquid extraction surface analysis-tandem mass spectrometry-based metabolomics for prediction of brain tumor relapse from sample-limited primary tissue archives. *Anal. Chem.* 93:6947–54
22. Sun N, Kunzke T, Sbiera S, Kircher S, Feuchtinger A, et al. 2019. Prognostic relevance of steroid sulfation in adrenocortical carcinoma revealed by molecular phenotyping using high-resolution mass spectrometry imaging. *Clin. Chem.* 65:1276–86
23. Sun N, Trajkovic-Arsic M, Li F, Wu Y, Münch C, et al. 2021. Native glycan fragments detected by MALDI mass spectrometry imaging are independent prognostic factors in pancreatic ductal adenocarcinoma. *EJNMMI Res.* 11:120
24. Orosco RK, Tapia VJ, Califano JA, Clary B, Cohen EEW, et al. 2018. Positive surgical margins in the 10 most common solid cancers. *Sci. Rep.* 8:5686
25. Yang X, Song X, Zhang X, Shankar V, Wang S, et al. 2021. *In situ* DESI-MSI lipidomic profiles of mucosal margin of oral squamous cell carcinoma. *EBioMedicine* 70:103529
26. Vijayalakshmi K, Shankar V, Bain RM, Nolley R, Sonn GA, et al. 2020. Identification of diagnostic metabolic signatures in clear cell renal cell carcinoma using mass spectrometry imaging. *Int. J. Cancer* 147:256–65
27. Brown HM, Alfaro CM, Pirro V, Cooks RG, Dey M, et al. 2021. Intraoperative mass spectrometry platform for IDH mutation status prediction, glioma diagnosis, and estimation of tumor cell infiltration. *J. Appl. Lab. Med.* 6:902–16
28. Alfaro CM, Pirro V, Keating MF, Hattab EM, Cooks RG, Cohen-Gadol AA. 2020. Intraoperative assessment of isocitrate dehydrogenase mutation status in human gliomas using desorption electrospray ionization-mass spectrometry. *J. Neurosurg.* 132:180–87
29. Margulis K, Chiou AS, Aasi SZ, Tibshirani RJ, Tang JY, Zare RN. 2018. Distinguishing malignant from benign microscopic skin lesions using desorption electrospray ionization mass spectrometry imaging. *PNAS* 115:6347–52
30. Chen X, Gao J, Wang T, Jiang X, Chen J, et al. 2019. Hepatocarcinoma discrimination by ratiometric lipid profiles using tip-contact sampling/ionization mass spectrometry. *Anal. Chem.* 91:10376–80
31. Basu SS, Stopka SA, Abdelmoula WM, Randall EC, Gimenez-Cassina Lopez B, et al. 2021. Interim clinical trial analysis of intraoperative mass spectrometry for breast cancer surgery. *NPJ Breast Cancer* 7:116

32. Huang YC, Chung HH, Dutkiewicz EP, Chen CL, Hsieh HY, et al. 2020. Predicting breast cancer by paper spray ion mobility spectrometry mass spectrometry and machine learning. *Anal. Chem.* 92:1653–57
33. Kiritani S, Yoshimura K, Arita J, Kokudo T, Hakoda H, et al. 2021. A new rapid diagnostic system with ambient mass spectrometry and machine learning for colorectal liver metastasis. *BMC Cancer* 21:262
34. Giordano S, Takeda S, Donadon M, Saiki H, Brunelli L, et al. 2020. Rapid automated diagnosis of primary hepatic tumour by mass spectrometry and artificial intelligence. *Liver Int*. 40:3117–24
35. Basu SS, Regan MS, Randall EC, Abdelmoula WM, Clark AR, et al. 2019. Rapid MALDI mass spectrometry imaging for surgical pathology. *NPJ Precis. Oncol.* 3:17
36. Vaysse PM, Grabsch HI, van den Hout M, Bemelmans MHA, Heeren RMA, et al. 2021. Real-time lipid patterns to classify viable and necrotic liver tumors. *Lab. Investig.* 101:381–95
37. Tzafetas M, Mitra A, Paraskevaidi M, Bodai Z, Kalliala I, et al. 2020. The intelligent knife (iKnife) and its intraoperative diagnostic advantage for the treatment of cervical disease. *PNAS* 117:7338–46
38. Van Hese L, De Vleeschouwer S, Theys T, Lariviere E, Solie L, et al. 2022. Towards real-time intraoperative tissue interrogation for REIMS-guided glioma surgery. *J. Mass Spectrom. Adv. Clin. Lab.* 24:80–89
39. Vaysse PM, Demers I, van den Hout M, van de Worp W, Anthony IGM, et al. 2022. Evaluation of the sensitivity of metabolic profiling by rapid evaporative ionization mass spectrometry: toward more radical oral cavity cancer resections. *Anal. Chem.* 94:6939–47
40. Vaysse PM, Kooreman LFS, Engelen SME, Kremer B, Olde Damink SWM, et al. 2020. Stromal vapors for real-time molecular guidance of breast-conserving surgery. *Sci. Rep.* 10:20109
41. Zhang J, Sans M, DeHoog RJ, Garza KY, King ME, et al. 2021. Clinical translation and evaluation of a handheld and biocompatible mass spectrometry probe for surgical use. *Clin. Chem.* 67:1271–80
42. King ME, Zhang J, Lin JQ, Garza KY, DeHoog RJ, et al. 2021. Rapid diagnosis and tumor margin assessment during pancreatic cancer surgery with the MasSpec Pen technology. *PNAS* 118:e2104411118
43. Saudemont P, Quanico J, Robin YM, Baud A, Balog J, et al. 2018. Real-time molecular diagnosis of tumors using water-assisted laser desorption/ionization mass spectrometry technology. *Cancer Cell* 34:840–51.e4
44. Ogrinc N, Kruszewski A, Chaillou P, Saudemont P, Lagadec C, et al. 2021. Robot-assisted SpiderMass for *in vivo* real-time topography mass spectrometry imaging. *Anal. Chem.* 93:14383–91
45. Ogrinc N, Attencourt C, Colin E, Boudahi A, Tebbakha R, et al. 2022. Mass spectrometry-based differentiation of oral tongue squamous cell carcinoma and nontumor regions with the SpiderMass technology. *Front. Oral Health* 3:827360
46. Woolman M, Kuzan-Fischer CM, Ferry I, Kiyota T, Luu B, et al. 2019. Picosecond infrared laser desorption mass spectrometry identifies medulloblastoma subgroups on intrasurgical timescales. *Cancer Res.* 79:2426–34
47. Woolman M, Qiu J, Kuzan-Fischer CM, Ferry I, Dara D, et al. 2020. In situ tissue pathology from spatially encoded mass spectrometry classifiers visualized in real time through augmented reality. *Chem. Sci.* 11:8723–35
48. Keating MF, Zhang J, Feider CL, Retailleau S, Reid R, et al. 2020. Integrating the MasSpec pen to the da Vinci surgical system for *in vivo* tissue analysis during a robotic assisted porcine surgery. *Anal. Chem.* 92:11535–42
49. Mason S, Manoli E, Poynter L, Alexander J, Paizs P, et al. 2020. Mass spectrometry transanal minimally invasive surgery (MS-TAMIS) to promote organ preservation in rectal cancer. *Surg. Endosc.* 34:3618–25
50. Manoli E, Mason S, Ford L, Adebesin A, Bodai Z, et al. 2021. Validation of ultrasonic harmonic scalpel for real-time tissue identification using rapid evaporative ionization mass spectrometry. *Anal. Chem.* 93:5906–16
51. Michno W, Nyström S, Wehrli P, Lashley T, Brinkmalm G, et al. 2019. Pyroglutamation of amyloid-βx-42 (Aβx-42) followed by Aβ1–40 deposition underlies plaque polymorphism in progressing Alzheimer's disease pathology. *J. Biol. Chem.* 294:6719–32
52. Michno W, Wehrli PM, Koutarapu S, Marsching C, Minta K, et al. 2022. Structural amyloid plaque polymorphism is associated with distinct lipid accumulations revealed by trapped ion mobility mass spectrometry imaging. *J. Neurochem.* 160:482–98

53. Akerman SC, Hossain S, Shobo A, Zhong Y, Jourdain R, et al. 2019. Neurodegenerative disease-related proteins within the epidermal layer of the human skin. *J. Alzheimer's Dis.* 69:463–78
54. Sisley EK, Hale OJ, Styles IB, Cooper HJ. 2022. Native ambient mass spectrometry imaging of ligand-bound and metal-bound proteins in rat brain. *J. Am. Chem. Soc.* 144:2120–28
55. Hawkinson TR, Clarke HA, Young LEA, Conroy LR, Markussen KH, et al. 2022. In situ spatial glycomic imaging of mouse and human Alzheimer's disease brains. *Alzheimer's Dement*. 18:1721–35
56. Pang X, Gao S, Ga M, Zhang J, Luo Z, et al. 2021. Mapping metabolic networks in the brain by ambient mass spectrometry imaging and metabolomics. *Anal. Chem.* 93:6746–54
57. Vallianatou T, Shariatgorji R, Nilsson A, Karlgren M, Hulme H, et al. 2021. Integration of mass spectrometry imaging and machine learning visualizes region-specific age-induced and drug-target metabolic perturbations in the brain. *ACS Chem. Neurosci.* 12:1811–23
58. Vos DRN, Bowman AP, Heeren RMA, Balluff B, Ellis SR. 2019. Class-specific depletion of lipid ion signals in tissues upon formalin fixation. *Int. J. Mass Spectrom.* 446:116212
59. Harris A, Roseborough A, Mor R, Yeung KKC, Whitehead SN. 2020. Ganglioside detection from formalin-fixed human brain tissue utilizing MALDI imaging mass spectrometry. *J. Am. Soc. Mass Spectrom.* 31:479–87
60. Pinsky W, Harris A, Roseborough AD, Wang W, Khan AR, et al. 2021. Regional lipid expression abnormalities identified using MALDI IMS correspond to MRI-defined white matter hyperintensities within post-mortem human brain tissues. *Anal. Chem.* 93:2652–59
61. Ajith A, Mondal S, Chattopadhyay S, Kumar A, Sthanikam Y, et al. 2021. Mass spectrometry imaging deciphers dysregulated lipid metabolism in the human hippocampus affected by temporal lobe epilepsy. *ACS Chem. Neurosci.* 12:4187–94
62. Tanaka E, Ogawa Y, Fujii R, Shimonaka T, Sato Y, et al. 2020. Metabolomic analysis and mass spectrometry imaging after neonatal stroke and cell therapies in mouse brains. *Sci. Rep.* 10:21881
63. Liu X, Liu R, Fu D, Wu H, Zhao X, et al. 2021. Dl-3-n-butylphthalide inhibits neuroinflammation by stimulating foxp3 and Ki-67 in an ischemic stroke model. *Aging* 13:3763–78
64. Mallah K, Quanico J, Raffo-Romero A, Cardon T, Aboulouard S, et al. 2019. Matrix-assisted laser desorption/ionization-mass spectrometry imaging of lipids in experimental model of traumatic brain injury detecting acylcarnitines as injury related markers. *Anal. Chem.* 91:11879–87
65. Havlikova J, May RC, Styles IB, Cooper HJ. 2021. Liquid extraction surface analysis mass spectrometry of ESKAPE pathogens. *J. Am. Soc. Mass Spectrom.* 32:1345–51
66. Cameron SJS, Bodai Z, Temelkuran B, Perdones-Montero A, Bolt F, et al. 2019. Utilisation of ambient laser desorption ionisation mass spectrometry (ALDI-MS) improves lipid-based microbial species level identification. *Sci. Rep.* 9:3006
67. Bardin EE, Cameron SJS, Perdones-Montero A, Hardiman K, Bolt F, et al. 2018. Metabolic phenotyping and strain characterisation of *Pseudomonas aeruginosa* isolates from cystic fibrosis patients using rapid evaporative ionisation mass spectrometry. *Sci. Rep.* 8:10952
68. Schultz D, Cuypers F, Skorka SB, Rockstroh J, Gesell Salazar M, et al. 2022. Bioactive lipid screening during respiratory tract infections with bacterial and viral pathogens in mice. *Metabolomics* 18:39
69. Havlikova J, May RC, Styles IB, Cooper HJ. 2020. Direct identification of bacterial and human proteins from infected wounds in living 3D skin models. *Sci. Rep.* 10:11900
70. Ryan DJ, Patterson NH, Putnam NE, Wilde AD, Weiss A, et al. 2019. MicroLESA: integrating autofluorescence microscopy, in situ micro-digestions, and liquid extraction surface analysis for high spatial resolution targeted proteomic studies. *Anal. Chem.* 91:7578–85
71. Guiberson ER, Weiss A, Ryan DJ, Monteith AJ, Sharman K, et al. 2021. Spatially targeted proteomics of the host–pathogen interface during staphylococcal abscess formation. *ACS Infect. Dis.* 7:101–13
72. Povilaitis SC, Chakraborty A, Kirkpatrick LM, Downey RD, Hauger SB, Eberlin LS. 2022. Identifying clinically relevant bacteria directly from culture and clinical samples with a handheld mass spectrometry probe. *Clin. Chem.* 68:1459–70
73. Margulis K, Zhou Z, Fang Q, Sievers RE, Lee RJ, Zare RN. 2018. Combining desorption electrospray ionization mass spectrometry imaging and machine learning for molecular recognition of myocardial infarction. *Anal. Chem.* 90:12198–206

74. Van Nuffel S, Quatredeniers M, Pirkl A, Zakel J, Le Caer JP, et al. 2020. Multimodal imaging mass spectrometry to identify markers of pulmonary arterial hypertension in human lung tissue using MALDI-ToF, ToF-SIMS, and hybrid SIMS. *Anal. Chem.* 92:12079–87
75. Lou JQ, Cao Y, Yu YJ, Hu L, Mao ZS, et al. 2020. Investigation of heart lipid changes in acute β-AR activation-induced sudden cardiac death by time-of-flight secondary ion mass spectrometry. *Analyst* 145:5889–96
76. Johno H, Yoshimura K, Mori Y, Kimura T, Niimi M, et al. 2018. Detection of potential new biomarkers of atherosclerosis by probe electrospray ionization mass spectrometry. *Metabolomics* 14:38
77. Davies HA, Caamano-Gutierrez E, Sarsby J, Nawaytou O, Harky A, et al. 2021. Exploring the potential of rapid evaporative ionization mass spectrometry (Intelligent Knife) for point-of-care testing in aortic surgery. *Eur. J. Cardiothorac. Surg.* 60:562–68
78. Davies HA, Caamano-Gutierrez E, Sarsby J, Chim YH, Barrett S, et al. 2022. Rapid evaporative ionization mass spectrometry (intelligent knife) for point-of-care testing in acute aortic dissection surgery. *Interact. Cardiovasc. Thorac. Surg.* 34:833–40
79. Feider CL, Woody S, Ledet S, Zhang J, Sebastian K, et al. 2019. Molecular imaging of endometriosis tissues using desorption electrospray ionization mass spectrometry. *Sci. Rep.* 9:15690
80. Lin M, Eberlin LS, Seeley EH. 2022. Reduced hemoglobin signal and improved detection of endogenous proteins in blood-rich tissues for MALDI mass spectrometry imaging. *J. Am. Soc. Mass Spectrom.* 33:296–303
81. Müller R, Henss A, Kampschulte M, Rohnke M, Langheinrich AC, et al. 2019. Analysis of microscopic bone properties in an osteoporotic sheep model: a combined biomechanics, FE and ToF-SIMS study. *J. R. Soc. Interface* 16:20180793
82. Rocha B, Cillero-Pastor B, Ruiz-Romero C, Paine MRL, Canete JD, et al. 2021. Identification of a distinct lipidomic profile in the osteoarthritic synovial membrane by mass spectrometry imaging. *Osteoarthritis Cartilage* 29:750–61
83. Eveque-Mourroux MR, Emans PJ, Zautsen RRM, Boonen A, Heeren RMA, Cillero-Pastor B. 2019. Spatially resolved endogenous improved metabolite detection in human osteoarthritis cartilage by matrix assisted laser desorption ionization mass spectrometry imaging. *Analyst* 144:5953–58
84. Celis R, Cuervo A, Ramirez J, Canete JD. 2019. Psoriatic synovitis: singularity and potential clinical implications. *Front. Med.* 6:14
85. Nauta SP, Poeze M, Heeren RMA, Porta Siegel T. 2020. Clinical use of mass spectrometry (imaging) for hard tissue analysis in abnormal fracture healing. *Clin. Chem. Lab. Med.* 58:897–913
86. Khodjaniyazova S, Hanne NJ, Cole JH, Muddiman DC. 2019. Mass spectrometry imaging (MSI) of fresh bones using infrared matrix-assisted laser desorption electrospray ionization (IR-MALDESI). *Anal. Methods* 11:5929–38
87. Good CJ, Neumann EK, Butrico CE, Cassat JE, Caprioli RM, Spraggins JM. 2022. High spatial resolution MALDI imaging mass spectrometry of fresh-frozen bone. *Anal. Chem.* 94:3165–72
88. Genangeli M, Heeren RMA, Porta Siegel T. 2019. Tissue classification by rapid evaporative ionization mass spectrometry (REIMS): comparison between a diathermic knife and CO_2 laser sampling on classification performance. *Anal. Bioanal. Chem.* 411:7943–55
89. Prentice BM, Hart NJ, Phillips N, Haliyur R, Judd A, et al. 2019. Imaging mass spectrometry enables molecular profiling of mouse and human pancreatic tissue. *Diabetologia* 62:1036–47
90. Zhang G, Zhang J, DeHoog RJ, Pennathur S, Anderton CR, et al. 2020. DESI-MSI and METASPACE indicates lipid abnormalities and altered mitochondrial membrane components in diabetic renal proximal tubules. *Metabolomics* 16:11
91. Wang Z, Fu W, Huo M, He B, Liu Y, et al. 2021. Spatial-resolved metabolomics reveals tissue-specific metabolic reprogramming in diabetic nephropathy by using mass spectrometry imaging. *Acta Pharm. Sin. B* 11:3665–77
92. Banerjee S, Wong AC, Yan X, Wu B, Zhao H, et al. 2019. Early detection of unilateral ureteral obstruction by desorption electrospray ionization mass spectrometry. *Sci. Rep.* 9:11007
93. Palmer A, Phapale P, Chernyavsky I, Lavigne R, Fay D, et al. 2017. FDR-controlled metabolite annotation for high-resolution imaging mass spectrometry. *Nat. Methods* 14:57–60

94. Ivanova M, Dyadyk O, Ivanov D, Clerici F, Smith A, Magni F. 2020. Matrix-assisted laser desorption/ionization mass spectrometry imaging to uncover protein alterations associated with the progression of IgA nephropathy. *Virchows Arch*. 476:903–14
95. Smith A, Iablokov V, Mazza M, Guarnerio S, Denti V, et al. 2020. Detecting proteomic indicators to distinguish diabetic nephropathy from hypertensive nephrosclerosis by integrating matrix-assisted laser desorption/ionization mass spectrometry imaging with high-mass accuracy mass spectrometry. *Kidney Blood Press Res*. 45:233–48
96. de Boer IH, Alpers CE, Azeloglu EU, Balis UG, Barasch JM, et al. 2021. Rationale and design of the kidney precision medicine project. *Kidney Int*. 99:498–510
97. Hansen J, Sealfon R, Menon R, Eadon MT, Lake BB, et al. 2022. A reference tissue atlas for the human kidney. *Sci. Adv.* 8:eabn4965
98. Feenstra AD, Dueñas ME, Lee YJ. 2017. Five micron high resolution MALDI mass spectrometry imaging with simple, interchangeable, multi-resolution optical system. *J. Am. Soc. Mass Spectrom.* 28:434–42
99. Norris JL, Caprioli RM. 2013. Analysis of tissue specimens by matrix-assisted laser desorption/ionization imaging mass spectrometry in biological and clinical research. *Chem. Rev.* 113:2309–42
100. Ščupáková K, Balluff B, Tressler C, Adelaja T, Heeren RMA, et al. 2020. Cellular resolution in clinical MALDI mass spectrometry imaging: the latest advancements and current challenges. *J. Clin. Chem. Lab. Med.* 58:914–29
101. Engel KM, Prabutzki P, Leopold J, Nimptsch A, Lemmnitzer K, et al. 2022. A new update of MALDI-TOF mass spectrometry in lipid research. *Prog. Lipid Res.* 86:101145
102. Drake RR, West CA, Mehta AS, Angel PM. 2018. MALDI mass spectrometry imaging of N-linked glycans in tissues. In *Glycobiophysics*, ed. Y Yamaguchi, K Kato, pp. 59–76. Singapore: Springer
103. Kubicek M, Holzlechner G, Opitz AK, Larisegger S, Hutter H, Fleig J. 2014. A novel ToF-SIMS operation mode for sub 100 nm lateral resolution: application and performance. *Appl. Surface Sci.* 289:407–16
104. Sodhi RNS. 2004. Time-of-flight secondary ion mass spectrometry (TOF-SIMS):—versatility in chemical and imaging surface analysis. *Analyst* 129:483–87
105. Yoon S, Lee TG. 2018. Biological tissue sample preparation for time-of-flight secondary ion mass spectrometry (ToF–SIMS) imaging. *Nano Converg.* 5:24
106. Noun M, Akoumeh R, Abbas I. 2022. Cell and tissue imaging by TOF-SIMS and MALDI-TOF: an overview for biological and pharmaceutical analysis. *Microsc. Microanal.* 28:1–26
107. Lv Y, Li T, Guo C, Sun C, Tang F, et al. 2019. A high-performance bio-tissue imaging method using air flow-assisted desorption electrospray ionization coupled with a high-resolution mass spectrometer. *Chin. Chem. Lett.* 30:461–64
108. Luo Z, He J, Chen Y, He J, Gong T, et al. 2013. Air flow-assisted ionization imaging mass spectrometry method for easy whole-body molecular imaging under ambient conditions. *Anal. Chem.* 85:2977–82
109. He J, Sun C, Li T, Luo Z, Huang L, et al. 2018. A sensitive and wide coverage ambient mass spectrometry imaging method for functional metabolites based molecular histology. *Adv. Sci.* 5:1800250
110. Quartier J, Rao W, Slade S, Métral F, Lapteva M, Kalia YN. 2021. DESI-MS imaging to visualize spatial distribution of xenobiotics and endogenous lipids in the skin. *Int. J. Pharm.* 607:120967
111. Holm NB, Deryabina M, Knudsen CB, Janfelt C. 2022. Tissue distribution and metabolic profiling of cyclosporine (CsA) in mouse and rat investigated by DESI and MALDI mass spectrometry imaging (MSI) of whole-body and single organ cryo-sections. *Anal. Bioanal. Chem.* 414:7167–77
112. Takats Z, Wiseman JM, Gologan B, Cooks RG. 2004. Mass spectrometry sampling under ambient conditions with desorption electrospray ionization. *Science* 306:471–73
113. Soudah T, Zoabi A, Margulis K. 2023. Desorption electrospray ionization mass spectrometry imaging in discovery and development of novel therapies. *Mass Spectrom. Rev.* 42:751–78
114. Das S, Bhatia R. 2022. Liquid extraction surface analysis-mass spectrometry: an advanced and environment-friendly analytical tool in modern analysis. *J. Sep. Sci.* 45:2746–65
115. Kertesz V, Van Berkel GJ. 2010. Fully automated liquid extraction-based surface sampling and ionization using a chip-based robotic nanoelectrospray platform. *J. Mass Spectrom.* 45:252–60

116. Wu Q, Huang ZH, Wang Y, Zhang ZM, Lu HM. 2020. Absolute quantitative imaging of sphingolipids in brain tissue by exhaustive liquid microjunction surface sampling-liquid chromatography-mass spectrometry. *J. Chromatogr. A* 1609:460436
117. Simon D, Oleschuk R. 2021. The liquid micro junction-surface sampling probe (LMJ-SSP); a versatile ambient mass spectrometry interface. *Analyst* 146:6365–78
118. Van Berkel GJ, Kertesz V, Koeplinger KA, Vavrek M, Kong A-NT. 2008. Liquid microjunction surface sampling probe electrospray mass spectrometry for detection of drugs and metabolites in thin tissue sections. *J. Mass Spectrom.* 43:500–8
119. Yin R, Burnum-Johnson KE, Sun X, Dey SK, Laskin J. 2019. High spatial resolution imaging of biological tissues using nanospray desorption electrospray ionization mass spectrometry. *Nat. Protoc.* 14:3445–70
120. Hale OJ, Hughes JW, Sisley EK, Cooper HJ. 2022. Native ambient mass spectrometry enables analysis of intact endogenous protein assemblies up to 145 kDa directly from tissue. *Anal. Chem.* 94:5608–14
121. Roach PJ, Laskin J, Laskin A. 2010. Nanospray desorption electrospray ionization: an ambient method for liquid-extraction surface sampling in mass spectrometry. *Analyst* 135:2233–36
122. Zhang J, Rector J, Lin JQ, Young JH, Sans M, et al. 2017. Nondestructive tissue analysis for ex vivo and in vivo cancer diagnosis using a handheld mass spectrometry system. *Sci. Transl. Med.* 9. **https://doi.org/10.1126/scitranslmed.aan3968**
123. Woolman M, Gribble A, Bluemke E, Zou J, Ventura M, et al. 2017. Optimized mass spectrometry analysis workflow with polarimetric guidance for ex vivo and in situ sampling of biological tissues. *Sci. Rep.* 7:468
124. Schäfer K-C, Dénes J, Albrecht K, Szaniszló T, Balog J, et al. 2009. In vivo, in situ tissue analysis using rapid evaporative ionization mass spectrometry. *Angew. Chem. Int. Ed.* 48:8240–42
125. Fatou B, Saudemont P, Leblanc E, Vinatier D, Mesdag V, et al. 2016. In vivo real-time mass spectrometry for guided surgery application. *Sci. Rep.* 6:25919